Dynamical multicluster model for electroweak and charge-exchange reactions

B. V. Danilin and M. V. Zhukov
The Kurchatov Institute of Atomic Energy, Moscow, U.S.S.R.

S. N. Ershov, F. A. Gareev, and R. S. Kurmanov
Joint Institute for Nuclear Research, Dubna, 101000 Moscow, U.S.S.R.

J. S. Vaagen
Institute of Physics, University of Bergen, Bergen, Norway

J. M. Bang
The Niels Bohr Institute, Copenhagen, Denmark
(Received 26 December 1990)

The hyperspherical harmonics method is used to solve the $\alpha+N+N$ three-body problem. The resulting wave functions and corresponding densities are, with satisfactory result, tested against a variety of weak and electromagnetic data as well as nucleon-induced quasielastic reactions (p,p'), (n,p), and (p,n) on ^{6}Li as target. A procedure is outlined which generates reliable transition densities for the (projectile, ejectile) part of ^{6}Li-induced inelastic and charge-exchange reactions $A(^6\text{Li},b)B$, $b=^6\text{Li}^*$, ^{6}He, and ^{6}Be.

I. INTRODUCTION

Calculational procedures for lighter nuclei with pronounced multicluster features have now been developed which successfully reproduce a variety of observables for such systems. This coincides with increased experimental possibilities to make beams, both radioactive and exotic (such as ^{11}Li) of multicluster nuclei.

In this paper we present recent calculations for ^{6}Li, ^{6}He, and ^{6}Be within a formalism based on hyperspherical harmonics. Recent interest in charge-exchange reactions induced by ^{6}Li has accentuated the need for accurate transition densities (^{6}Li, ^{6}He) and (^{6}Li, ^{6}Be) if reliable information about the target-residual nuclei is to be extracted.

Charge-exchange reactions induced by ^{6}Li(g.s.; 1^+, $T=1$) have the following special features: (i) The (projectile, ejectile) overlap is maximal for (^{6}Li, ^{6}He) as reflected in the log(ft) values ($M_{if}^2=\text{const}/ft$) (see Table 1 in Ref. 1). (ii) In $^6\text{Li}\rightarrow{}^6\text{He}$ and $^6\text{Li}\rightarrow{}^6\text{Be}$ transitions, only the Gamow-Teller (GT) ($\Delta L=0$, $\Delta S=1$, and $\Delta T=1$) is allowed. Since the ^{6}Li and ^{6}He nuclei are very similar in structure, this GT transition is superallowed, with a minimal log(ft) value. (iii) Since the ^{6}He ejectile has only one long-lived state (0^+, $T=1$) and ^{6}Be one narrow resonant state (0^+, $T=1$), the ^{6}Li-induced reaction has an advantage compared with charge-exchange reactions induced by heavy ions, where many ejectile states usually are possible. (iv) Even starting from energies as low as $E(^6\text{Li})=10$ MeV/nucleon, the reaction can be described as a one-step process due to the loose binding in the system.

A large number of experimental and theoretical papers have been devoted to investigations of properties of the $A=6$ nuclei.[2] Keeping aside the history of the problem, there is strong evidence that a three-body $\alpha+2N$ model ($^6\text{Li}\rightarrow\alpha+n+p$, $^6\text{He}\rightarrow\alpha+n+n$, and $^6\text{Be}\rightarrow\alpha+p+p$) is sufficient to describe the main properties of $A=6$ nuclei (see, for example, Refs. 3–9).

In this model the intrinsic degrees of freedom are treated in an approximate way and pairwise NN and αN interactions fitted to experimental phase shifts and other experimental characteristics. Therefore, the six-particle task is reduced to the three-body problem with the Pauli principle treated in an approximate way. Eigenvalues and eigenfunctions are found by solving the dynamical Schrödinger or Faddeev equations. Nevertheless, up to now such a program with checks against weak and electromagnetic characteristics has only been carried out within the framework of variational calculations with projected Pauli forbidden states[3,7] and integral equation methods.[5,6]

In Ref. 9 a microscopic exploration of $A=6$, $J^\pi=0^+$ ($T=1$) nuclear states was carried out within the hyperspherical function method using the $\alpha+2N$ model with simple αN and NN potentials. Formalism of the method and some results are outlined in Ref. 9. The distinguishing feature of the method is a controlled accuracy of computations and great advantages connected with (i) the possibility of analytical calculations for most characteristics and corresponding physical transparency of the results. These facts are due to rotational and permutational invariance in the collective hyperradial variable; (ii) additional approximate symmetry in the dynamics (a single dominating hypermoment $K=2$,[9]; (iii) the possibility to include into the problem any realistic NN potential with repulsive core and tensor forces, and also more realistic l-dependent local αN potentials.[10]

Below, calculated wave functions are tested against a variety of electromagnetic and weak processes known with good accuracy. They are also used to study elastic and inelastic scattering of protons on ^{6}Li and charge-exchange reactions ^{6}Li$(p,n)^6$Be and ^{6}Li$(n,p)^6$He for a range of projectile energies.

II. STRUCTURE OF WAVE FUNCTIONS

In the $\alpha+2N$ model, the wave functions for the system $A=6$ are in the product form

$$\Phi^{\pi}_{JM}=\varphi_{\alpha}(\xi_{\alpha})\Psi^{T}_{JM}(\mathbf{x},\mathbf{y}) , \tag{1}$$

where φ_{α} is the α-particle intrinsic wave function ($J_{\alpha}=T_{\alpha}=0$), while Ψ^{T}_{JM} is the "active part" of the three-body wave function carrying the total angular momentum J, its projection M, and total isospin T. It depends on relative coordinates and nucleon spins (suppressed in our notation) and is the object of the calculation.

It is convenient to introduce translationally invariant normalized sets of Jacobi coordinates $\mathbf{x}$ and $\mathbf{y}$, say,

$$\mathbf{x}_3=(A_{12})^{1/2}\mathbf{r}_{12} , \tag{2}$$

$$\mathbf{y}_3=(A_{(12)3})^{1/2}\mathbf{r}_{(12)3} , \tag{3}$$

where $A_{12}=A_1A_2/(A_1+A_2)$ is the reduced mass number for the pair (1,2) and similarly for the c.m. of (1,2) with respect to particle 3. Notice that $\mathbf{x}_3$ is proportional to the relative coordinate within the pair (1,2), while $\mathbf{y}_3$ is colinear with the position of the c.m. of (1,2) with respect to 3, hence, also colinear with the c.m. coordinate of particle 3. For our special case we will use the labeling $1=N_1$, $2=N_2$, and $3=\alpha$. Alternative sets of Jacobi coordinates are obtained by cyclic permutations of (1,2,3).

In hyperspherical coordinates and LS representation, the wave function (WF) is given by

$$\Psi^{T}_{JM}(\mathbf{x},\mathbf{y})=\rho^{-5/2}\sum\chi^{LS}_{Kl_xl_y}(\rho)[\mathcal{Y}^{l_xl_y}_{KL}(\Omega_5)\otimes X_S]^{JM}X_{TM_T} , \tag{4}$$

where the hyperradius

$$\rho=(x^2+y^2)^{1/2}=[\tfrac{2}{3}(r^2_{12}+r^2_{23}+r^2_{31})]^{1/2}$$

is a collective rotationally and permutationally invariant variable. The hyperspherical polar angles are $\Omega_5=\{\theta,\hat{x},\hat{y}\}$ with $\theta=\arccos(y/\rho)$. $K=l_x+l_y+2n$ ($n=0,1,2,\ldots$) is the hypermoment and $X_{SM}(1,2)$ and $X_{TM}(1,2)$ the coupled spin and isospin functions. It should be noted, that every hyperharmonic in the shell-model language, corresponds to an infinite series of radial excitations.

Hyperspherical harmonics have the explicit form

$$\mathcal{Y}^{l_xl_y}_{KLM_L}(\Omega_5)=\Psi^{l_xl_y}_{K}(\theta)[Y_{l_x}(\hat{x})\otimes Y_{l_y}(\hat{y})]^{LM_L} , \tag{5}$$

$$\Psi^{l_xl_y}_{K}(\theta)=N^{l_xl_y}_{K}(\sin\theta)^{l_x}(\cos\theta)^{l_y}P^{l_x+1/2,l_y+1/2}_{n}(\cos2\theta) , \tag{6}$$

where $P^{\alpha,\beta}_n$ is the Jacobi polynomial, $N^{l_xl_y}_K$ a normalizing coefficient and $n=(K-l_x-l_y)/2$.

TABLE I. Depths (MeV) of the components of the αN potential.

	s	p	d	ls
$V^0_{\alpha N}$	50	−47.32	−23.00	−5.855

The wave function Ψ^{T}_{JM} is solution of the Schrödinger three-body equation:

$$(\hat{T}+\hat{V}-E)\Psi^{T}_{JM}=0, \quad \hat{V}=V_{\alpha N_1}+V_{\alpha N_2}+V_{N_1N_2} . \tag{7}$$

The $V_{\alpha N}$ potential was chosen with a p-wave component of Gaussian shape $V_0\exp[-(r^2/r_0^2)]$ and $\boldsymbol{l}\cdot\mathbf{s}$ force included,[11] and s- and d-wave Gaussian shape components with the same $r_0=2.35$ fm fitted from the phase-shift analysis of N-α scattering in the 0–25-MeV energy range. The depths of the potential are given in Table I. The Pauli principle was taken into account by a

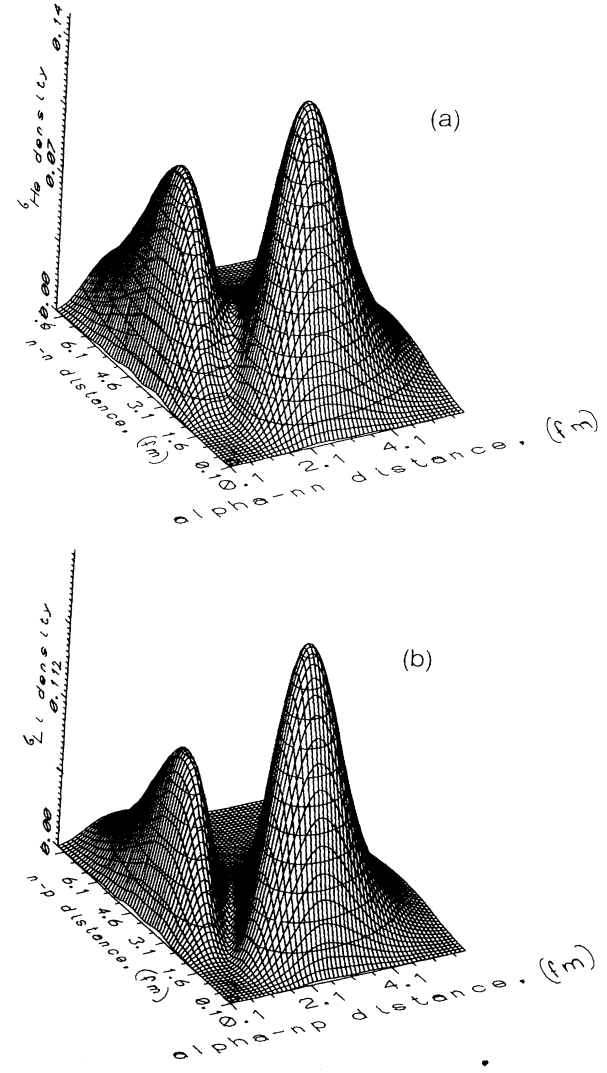

FIG. 1. Density distributions $P(r_{NN},r_{\alpha(NN)})$ (defined in the text) for the ground states of (a) ^{6}He and (b) ^{6}Li.

TABLE II. Weights (squared norms in %) of different ($LSl_x l_y$) components of $A=6$ states.

	$S=0$ $L=0$	$S=1$ $L=1$	$S=0$ $L=2$	$S=1$ $L=3$	$S=0$ $L=4$	$S=1$ $L=5$	$S=0$ $L=6$	$S=1$ $L=7$
^{6}He(0^+) $l_x=l_y=L$	82.87	13.96	2.31	0.69	0.58	0.06	0.002 6	0.000 52
^{6}Li(0^+) $l_x=l_y=L$	82.05	14.37	2.59	0.81	0.11	0.08	0.003 6	0.000 72
^{6}Be(0^+) $l_x=l_y=L$	78.53	17.22	2.99	1.09	0.81	0.09		

	$L=0$, $S=1$		$L=1$, $S=0$		$L=1$, $S=1$	$L=2$, $S=1$	
^{6}Li(1^+)	$l_x=0$ $l_y=0$	$l_x=2$ $l_y=2$	$l_x=1$ $l_y=1$	$l_x=3$ $l_y=3$	$l_x=2$ $l_y=2$	$l_x=0$ $l_y=2$	$l_x=2$ $l_y=0$
	91.93	1.11	3.23	0.11	0.24	0.28	3.10

repulsive s-wave αN potential. The NN interaction includes repulsion at small distance, $\boldsymbol{l}\cdot\mathbf{s}$, and tensor forces [the Gogny-Pires-DeTourreil (GPT) one].[12] The Coulomb part of the αN and NN interactions were treated in standard manner; details are given in Ref. 10. These types of interactions reproduce the binding energy of the 0^+ triplet and give a ground-state binding energy for ^{6}Li(1^+) to within 0.2 MeV (less bound) of the experimental value, 2.73 MeV.

The calculations were performed up to a $K_{\max}$ value large enough to stabilize the wave function and the binding energy. For ^{6}He ($l_x=l_y\leq 7$) it was found that the contributions from $l_x, l_y>3$ are negligible ($\sim 0.14\%$ of the norm) and also that the contributions from hypermomenta $K>6$ to the norm of the WF are small ($<10^{-2}$).

The lowest hyperharmonics with $K=0,2$ exhaust 95% of the norm (90% for $K=2$ only). This suggests that the hypermoment K is a "good" quantum number for many applications.

Table II gives the components (squared norms) of the wave functions for ^{6}He, ^{6}Li, and ^{6}Be. The WF of ^{6}Be(0^+) was calculated with a bound-state boundary condition.

Table III contains the geometrical characteristics (rms relative distances and radii) for the same wave functions and also for the excited 0^+ (3.56 MeV) of ^{6}Li. The matter radii are defined by

$$R^2_{\text{matter}}=\tfrac{1}{6}(2R_N^2+4R_\alpha^2+4\langle r_\alpha^2\rangle_{\text{matter}}) ,$$

with $\langle r_\alpha^2\rangle^{1/2}=1.49$ fm. The spatial structure of the WF for the ground states of ^{6}He and ^{6}Li is displayed in Figs. 1(a) and (b) by the density distribution

$$P(r_{NN}, r_{\alpha(NN)}) = r_{NN}^2 r_{\alpha(NN)}^2 \frac{1}{(2J+1)} \sum_M \int |\Psi^T_{JM}(\mathbf{x},\mathbf{y})|^2 d\hat{x}\, d\hat{y} . \quad (8)$$

In both cases two density peaks are present, corresponding to (i) a dinucleon configuration component with the two valence nucleons located together outside the α particle, and (ii) a cigarlike configuration with the valence nucleons positioned on opposite sides of the α particle.

The reason for these particle correlations, "Pauli focusing," is the Pauli principle which forbids the valence nucleons from occupying the $1s_{1/2}$ shell.[14] Qualitatively, similar results were obtained earlier by other authors[7] who employed a variational calculation with "Pauli blocking" included in the αN potentials.

To explore the spatial structure of, for example, the ^{6}He wave function, further, we switch off the NN interaction. As was to be expected, the dinucleon peak is now attenuated. The peak positions remain the same, but the peak heights are now nearly equal. An approximate analytic expression for the peak positions can be obtained if one assumes that the hypermoment $K=2$ is a "good" quantum number, and approximates the full wave function by the $K=2$, $L=0$, $S=l_x=l_y=0$ component. This results in a density which behaves as

TABLE III. Geometrical characteristics (rms radii) for ^{6}He(0^+), ^{6}Li* (0^+), ^{6}Be(0^+), and ^{6}Li(1^+). The quantities r_N and r_α are rms radii from the c.m. of the system.

	r_{NN} (fm)	$r_{\alpha N}$ (fm)	r_N (fm)	r_α (fm)	r_{mat} (fm)	$r^{\text{exp}}_{\text{mat}}$ (fm)
^{6}He	4.99	4.52	3.54	1.25	2.58	2.57±0.1[a]
^{6}Li*	5.30	4.70	3.70	1.29	2.66	
^{6}Be	6.14	5.12	4.11	1.36	2.87	
^{6}Li	3.80	4.06	3.06	1.20	2.35	2.45±0.1

[a]Recently, due to the availability of radioactive heavy-ion beams, a special investigation (Ref. 13) was carried out to extract an accurate matter radius for ^{6}He.

$$P(r_{NN},r_{\alpha(NN)})\simeq\sin^2(4\theta)\rho^4[\chi^{00}_{200}(\rho)]^2 , \tag{9}$$

and the positions of the maxima correspond to $\theta=\pi/8$ and $3\pi/8$ for fixed ρ_0. Taking into account the relations between r_{NN} and $r_{\alpha(NN)}$ and ρ,θ, one easily finds that $r^D_{NN}\simeq 0.54\rho_0$, $r^D_{\alpha(NN)}\simeq 0.80\rho_0$ for the dinucleon peak and $r^C_{NN}\simeq 1.3\rho_0$, $r^C_{\alpha(NN)}\simeq 0.33\rho_0$ for the cigarlike peak. The ratios $r_{NN}/r_{\alpha(NN)}$, respectively, 0.86 (D) and 3.94 (C) obtained from these simple estimates, are very close to the calculated values [see Fig. 1(a)].

III. COMPUTATIONAL PROCEDURE FOR TRANSITION DENSITIES

By definition, the transition density is given by

$$\rho^{JLS,T}_{fi}(r)=\langle J^fT^f\|\hat\rho\|J^iT^i\rangle=\left\langle J^fT^f\left|\left|\sum_k\frac{\delta(r-r_k)}{r_k^2}T_{LSJ}(k)\tau_T(k)\right|\right|J^iT^i\right\rangle , \tag{10}$$

where $T_{LSJ}(k)$ is a spherical tensor of the rank J,

$$T_{LSJM}(k)=\sum_{\mu\nu}\langle L\mu S\nu|JM\rangle Y_{L\mu}(\hat r_k)\sigma^S_\nu(k) , \tag{11}$$

which acts on the spin-angular coordinates of particle k. The diagonal ones ($f=i$) will just be referred to as densities. It is very convenient to calculate the transition densities in the "eigen" Jacobi coordinate system because of the colinearity of the c.m. coordinate $\mathbf{r}_k$ and the Jacobi coordinate $\mathbf{y}_k$, which are connected by the simple relation

$$\mathbf{r}_k=[(A_i+A_j)/AA_k]^{1/2}\mathbf{y}_k=a\mathbf{y}_k,\quad i,j,k=1,2,3 \tag{12}$$

with $A=A_i+A_j+A_k$ and cyclic permutations of (1,2,3). Hyperradial components $\chi(\rho)$ of the total wave function are invariant with respect to transitions from one Jacobi coordinate set to another. They transform via Raynal-Revai coefficients[15]

$$\mathcal{Y}^{l_{x_i}l_{y_i}}_{KLM_L}(\Omega^i_5)=\sum_{l_{x_j}l_{y_j}}\langle KLl_{x_i}l_{y_i}|KLl_{x_j}l_{y_j}\rangle\mathcal{Y}^{l_{x_j}l_{y_j}}_{KLM_L}(\Omega^j_5) . \tag{13}$$

Conservation of the quantum numbers K,L,M_L and parity implies the selection rule

$$l_{x_i}+l_{y_i}=l_{x_j}+l_{y_j}=\text{even} . \tag{14}$$

The spin-angular part of the reduced matrix element is well known and follows from standard tensor algebra

$$(-1)^{l^f_x+l^i_y-L^f-L+S^i+1-S}\cdot\hat L^i\hat L^f\hat S^i\hat S^f\hat J^i\hat J\cdot\delta(l^f_x,l^i_x)\times\begin{Bmatrix}l^i_y & l^i_x & L^i\\ L^f & L & l^f_y\end{Bmatrix}\begin{Bmatrix}\frac12 & \frac12 & S^i\\ S^f & S & \frac12\end{Bmatrix}\begin{Bmatrix}L^f & L^i & L\\ S^f & S^i & S\\ J^f & J^i & J\end{Bmatrix}\langle l^f_y\|Y_L\|l^i_y\rangle\langle\tfrac12\|\hat\sigma\|\tfrac12\rangle , \tag{15}$$

where $\hat A=(2A+1)^{1/2}$. The isospin reduced matrix of the $\hat\tau_T(1)$ operator can be expressed via the single-particle reduced matrix element $\langle\tau^f_1\|\hat\tau_T(1)\|\tau^i_1\rangle$ in usual manner:

$$\langle\tau^f_1\tau^f_2T^f|\hat\tau_T(1)|\tau^i_1\tau^i_2T^i\rangle=\delta(\tau^f_2,\tau^i_2)(-1)^{T_i+\tau^f_1+\tau^i_2-T}\cdot\hat T^f\hat T^i\begin{Bmatrix}\tau^i_1 & \tau^i_2 & T^i\\ T^f & T & \tau^f_1\end{Bmatrix}\langle\tau^f_1\|\hat\tau_T(1)\|\tau^i_1\rangle . \tag{16}$$

The spin- and isospin-reduced single-particle matrix element equals $(6)^{1/2}$. Reduced matrix elements and phases of the angular functions are defined according to Ref. 16.

Keeping in mind that the spin and isospin operators act on both nucleons, the full result is obtained by multiplying with the factor $[1+(-1)^{S^i+S^f+T^i+T^f}]$ obtained by a transposition $|12\rangle\rightarrow|21\rangle$ in the spin-isospin part of the wave function.

The radial matrix elements in (10) are reduced to one-dimensional integrals with varying lower limit (see Ref. 10):

$$\int\int\chi^f(x,y)[\delta(r-r_k)/r_k^2]\chi^i(x,y)y^2dy\,x^2dx =(1/a^3)\int_{r/a}^\infty\chi^f(\rho,\theta)\chi^i(\rho,\theta)[\rho^2-(r/a)^2]^{1/2}\rho^{-4}d\rho , \tag{17}$$

where

$$\chi^{i,j}(\rho,\theta)=\rho^{-5/2}\chi^{LS}_{Kl_x l_y}(\rho)\Psi_K^{l_x l_y}(\theta)$$

and (18)

$$\cos\theta=\frac{r}{a\rho} .$$

In addition to the operators (11), the full transition densities contain operators of the type $[Y_{j-1}(\hat{r}_k)L_1(k)]^{jm}$ which correspond to the convectional part of the current in electron sattering. But, for the transition densities $0^+\rightarrow 1^+$, with change in isospin $1\rightarrow 0$, these matrix elements are equal to zero. This result is easily obtained by invoking the specific symmetries of the formalism. To find the action on the individual nucleons we transform to the appropriate "eigen" Jacobi coordinate system, using even permutations. The hyperradial wave functions are invariant under such transformations, and hyperangular components are symmetrically transformed via Raynal-Revai coefficients. This leads to an overall multiplication factor $[1+(-1)^{T_f+T_i}]$ which is equal to zero for such transfers.

IV. TRANSITION DENSITIES

Numerical calculation has shown a power-law behavior r^ν of the transition densities $\rho^{JLS,T}(r)$ in the small-r region, where ν is close to the value 2 from naive shell model with two p-shell nucleons. A difference is, however, found in the density obtained by the three-body approach. From the shell model, the asymptotic behavior is expected to be

$$\rho(r)\sim\exp(-k_i r-k_f r)$$

consistent with single-particle asymptotics with

$$k_{i(f)}=\hbar^{-1}(\mu E_{i(f)})^{1/2} .$$

From Figs. 2(a) and (b) it is seen that the calculated densities are exponentially decreasing but with decay constant corresponding to a binding energy $\simeq 15$ MeV. This value is significantly greater than what would correspond to ^{6}He and ^{6}Li binding energies and is caused by the nucleon correlations and different asymptotics of the three-body wave functions.

Addressing the differences between the diagonal (matter, charge) ^{6}Li density and off-diagonal (transition) densities $^6\text{Li}\rightarrow{}^6\text{He}$ and $^6\text{Li}\rightarrow{}^6\text{Be}$, two seem to be present: (i) some difference in the asymptotic slope and (ii) the asymptotic magnitudes of the diagonal densities are different from off-diagonal ones. The latter was probably to be expected and can be explained in terms of a spectroscopic representation of the wave functions:

$$\begin{aligned}&\Psi(^6\text{Li})=\alpha(^3S_1)+\beta(^1P_1)+\gamma(^3D_1)+\delta(^3P_1) ,\\ &\alpha^2+\beta^2+\gamma^2+\delta^2=1 ,\\ &\Psi(^6\text{He})=A(^1S_0)+B(^3P_0) ,\\ &A^2+B^2=1 .\end{aligned} \tag{19}$$

From Eq. (10) we obtain

$$\begin{aligned}\rho(^6\text{Li})&=\rho^{000,0}\\ &=\alpha^2\langle{}^3S_1\|\hat{\rho}\|{}^3S_1\rangle+\beta^2\langle{}^1P_1\|\hat{\rho}\|{}^1P_1\rangle\\ &\quad+\gamma^2\langle{}^3D_1\|\hat{\rho}\|{}^3D_1\rangle+\delta^2\langle{}^3P_1\|\hat{\rho}\|{}^3P_1\rangle ,\end{aligned} \tag{20}$$

$$\begin{aligned}\rho(^6\text{Li}\rightarrow{}^6\text{He})&=\rho^{101,1}\\ &=[\alpha A\langle{}^3S_1\|\hat{\rho}|{}^1S_0\rangle\\ &\quad-\beta B(3)^{-1/2}\langle{}^1P_1\|\hat{\rho}\|{}^3P_0\rangle](3)^{-1/2} .\end{aligned} \tag{21}$$

It is obvious that $\rho^{000,0}$ would be significantly greater than $\rho^{101,1}$ if the signs of β and B were the same. But calculated amplitudes have opposite signs, caused by the

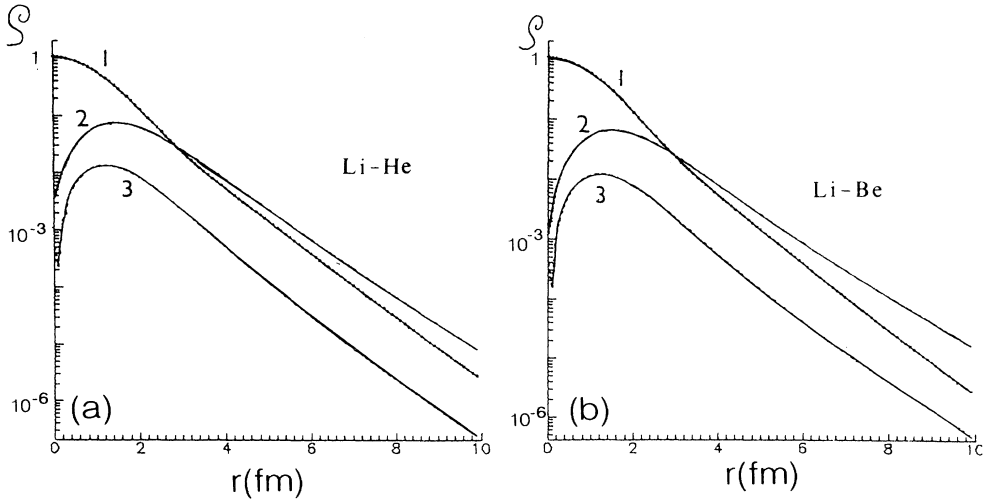

FIG. 2. Densities and transition densities in r space, for (a) $^6\text{Li}\rightarrow{}^6\text{He}$ and (b) $^6\text{Li}\rightarrow{}^6\text{Be}$. Curve 1, matter density for ^{6}Li; 2, transition density $\rho^{101,1}$; 3, transition density $\rho^{121,1}$.

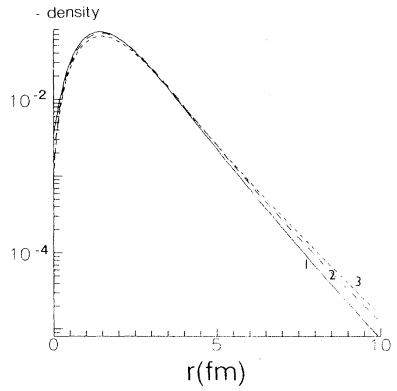

FIG. 3. Transition densities $\rho^{101,1}$ for 1, $\{^6\text{Li}\rightarrow{}^6\text{He}\}$; 2, $\{^6\text{Li(g.s.)}\rightarrow{}^6\text{Li}(0^+)\}$; and 3, $\{^6\text{Li(g.s.)}\rightarrow{}^6\text{Be}\}$.

spin-orbit splitting. Hence, the magnitude difference is due to (i) different magnitudes of β and B (ii) the lack of a $^3D_1$ component in the $\rho^{101,1}$ density, and (iii) additional suppression due to the geometry factor $(3)^{-1/2}$ in $\rho^{101,1}$. Furthermore, transition densities of the $^6\text{Li}\rightarrow{}^6\text{He}$, $^6\text{Li}\rightarrow{}^6\text{Be}$ and $^6\text{Li(g.s.)}\rightarrow{}^6\text{Li}(0^+)$ isotriplet with $T=1$ have somewhat different asymptotic behavior in r (Fig. 3) because of different binding energies and matter (charge) radii. It should be noted here that the 0^+ (1.37 MeV, $\Gamma=90$ keV) state of ^{6}Be has been calculated as a bound one, and the exact wave function can be of somewhat different form and value according to the general theorem for approximation of a quasistationary state by a bound state. (This state decays to the channel $p+p+\alpha$.) As a consequence, it can lead to a wider radial transition density $\rho(^6\text{Li}\rightarrow{}^6\text{Be})$ and narrower distribution of its Fourier component.

V. CALCULATIONS OF ELECTROMAGNETIC AND WEAK OBSERVABLES

A. Inelastic transverse $M1$ form factor of ^{6}Li

By the isospin selection rule, only the magnetic (spin) current contributes to the inelastic $M1$ form factor. The corresponding matrix element can be written in terms of the momentum-space transition densities $\rho^{101,1}(q)$ and $\rho^{121,1}(q)$,

$$F_T(q,M1)=(2\pi)^{1/2}Z^{-1}\hat{J}^{-1}\hat{J}_i^{-1}(2)^{3/2}q \times[-(3)^{-1/2}\rho^{121,1}(q)+(\tfrac{2}{3})^{1/2}\rho^{101,1}(q)] \times\left[\frac{g_s^p-g_s^n}{2}\right]f_p^c(q)/M\ , \tag{22}$$

where g_s^p (g_s^n) is the gyromagnetic factor of a proton (neutron) while $f_p^c(q)$ is the proton form factor taken in the dipole approximation. The $M1$ form factor is a superposition of transition densities which, in turn, depend on the correctness of the valence nucleon geometrical characteristics. These nucleons form a neutron "halo" in ^{6}He, responsible for a larger matter radius than in ^{6}Li. The magnitudes of the ρ are strongly influenced by the relative magnitudes of the different components in the ^{6}Li and ^{6}He wave functions. In the spectroscopic notations (19), $\rho^{101,1}$ is defined by (21) while

$$\rho^{121,1}=(5)^{1/2}\beta B\langle{}^3P_0\|\hat{\rho}\|{}^1P_1\rangle +2(3)^{1/2}\gamma A\langle{}^1S_0\|\hat{\rho}\|{}^3D_1\rangle +3(\tfrac{3}{2})^{1/2}\gamma B\langle{}^3P_0\|\hat{\rho}\|{}^3D_1\rangle\ . \tag{23}$$

The components of the wave function are intimately connected with the dynamics of the system; the P component depends on the spin-orbit αN force, and the D component mainly on the NN tensor force.

In Fig. 4 the calculated $M1$ form factor is compared with experimental data.[17] The theoretical curve reproduces the location of the minimum and part of the second maximum up to $q\leq 2$ fm^{-1}. As for most nuclei, the second maximum is underestimated for $q>2$ fm^{-1} since well-known contributions from relativistic corrections and mesonic exchange currents, essential in this region, have been left out. Almost the same conclusions are arrived at for the elastic $M1$ form factor. The contribution from the orbital current is very small $\simeq 5\%$ and its magnitude is similar to the orbital contribution to the magnetic moment.

To comment on the sensitivity of the $M1$ form factor to the NN tensor force, we mention that, in spite of the binding energy and geometrical characteristics being well reproduced in calculations with purely central NN forces, the minimum location of the $M1$ inelastic form factor is shifted to $q=1.6$ fm^{-1} and the second maximum is significantly less than with a tensor force. It should be noted that our result is very close to that of Ref. 18, obtained by a variational method (but only after additional *a posteriori* antisymmetrization of the total WF). It differs drastically from the result of an integral equation method.[6]

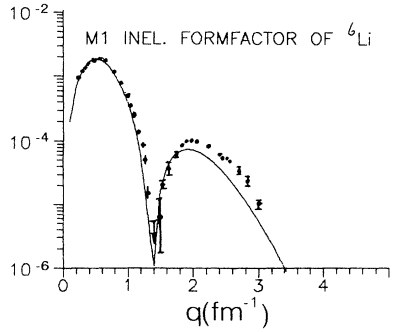

FIG. 4. The inelastic transverse $M1$ form factor of ^{6}Li. Experimental data are taken from Ref. 17.

TABLE IV. Calculated and experimental ^{6}Li magnetic moments.

	μ^l_{NN}	μ^l_α	μ^s_{NN}	$\mu_{\rm tot}$
Theory	0.0417	0.0071	0.7946	0.8433
Expt.				0.822

B. ^{6}Li(g.s.) magnetic moment

In the standard nonrelativistic approximation the calculated magnetic moment

$$\mu=\langle JJ|\hat{\mu}_z|JJ\rangle\ ,$$
$$\hat{\boldsymbol{\mu}}^{\,l}=\sum_i (e\hbar/2M_ic)g_l^i\mathbf{L}(i)\ , \tag{24}$$
$$\hat{\boldsymbol{\mu}}^{\,s}=\sum_i (e\hbar/2M_ic)\tfrac{1}{2}g_s^i\boldsymbol{\sigma}(i)$$

(without spin-orbit, relativistic, and mesonic exchange current corrections) is very close to that obtained in the integral equation method[19] and coincides with experimental value within 2.5% (see Table IV). From Table IV it is seen that the magnetic moment is mainly determined by its spin part ($\simeq$95%). Some sensitivity (like for the $M1$ form factor) to the tensor component of the NN potential is, however, present.

C. $M1$ radiative width of ^{6}Li

The radiative width of the ^{6}Li $M1$ transition

$$0^+(3.56\ \text{MeV})\rightarrow 1^+(\text{g.s.})$$

is defined by the transverse $M1$ form factor value at the photonic point

$$\Gamma_\gamma=2\pi Z^2\alpha[(2J_i+1)/(2J_f+1)]E_x|F_T(q)|^2\ , \tag{25}$$

where E_x is the energy of the $0^+\rightarrow 1^+$ transition. The calculated value $\Gamma_\gamma=8.13$ eV coincides within experimental errors with the measured value $\Gamma_\gamma=8.2\pm0.2$ eV. It should be pointed out that $F_T^2(q)$ at the photonic point can be expressed with an accuracy of $\sim q^2\sim 10^{-4}$ by the Gamow-Teller matrix element of ^{6}He.

D. ^{6}He β decay

In the expression for the ft value

$$ft=2ft(0^+\rightarrow 0^+)/[(g_A/g_V)^2B(\text{GT})]\ , \tag{26}$$

we used $ft(0^+\rightarrow 0^+)=3072.4\pm1.6$ sec.[20] Taking into account uncertainties in $\lambda=g_A/g_V$, the obtained value is $ft=776.3\pm2.5$ ($\beta_{\rm GT}=4.923$) for $\lambda=-1.268\pm0.002$ (Ref. 21) from neutron β decay; close to experiment ($ft_{\rm exp}=812.8\pm3.8$). The calculation with central NN force only gives a result which is 12 units less than given above. This fact once more stresses that the NN tensor forces play a significant role in the $\alpha+2N$ dynamics. (The ft value is insensitive to the $\boldsymbol{l}\cdot\mathbf{s}$ component of the αN forces.) The difference between experimental and theoretical ft values indicates a possible renormalization of the axial-vector weak constant λ (taking into account our good description of $M1$ inelastic form factors) to a value $\tilde{\lambda}=-1.24$, which is consistent with the trend in $g_{\rm axial}(\lambda)$ value in nuclear matter.

In conclusion we find good agreement with experimental data for electromagnetic and weak properties of low-lying states of $A=6$ nuclei which depend on dynamics of the system and can be expressed in terms of transition densities. In particular, we emphasize the $M1$ inelastic form factor. On this basis we now proceed to study charge-exchange transition densities for the isotriplet.

VI. QUASIELASTIC SCATTERING OF NUCLEONS ON ^{6}Li

Unlike the weak and electromagnetic processes which are well understood from a theoretical point of view, the description of quasielastic reactions of nucleons on nuclei contains a large number of assumptions where at least some require a better justification from first principle. In the intermediate-energy region and for small transferred momenta, the description is somewhat simplified, implying a decreased number of approximations and a corresponding increase in the reliability of the theoretical analysis.

Therefore, we restrict ourselves by investigating the reactions ^{6}Li$(p,n)^6$Be, ^{6}Li$(n,p)^6$He, and ^{6}Li$(p,p')^6$Li$(0^+,3.56$ MeV) at energies larger than 100 MeV. In this energy region at small-momentum transfer, the dynamics of the process can be described as a single-step transition and the theoretical analysis can be carried out in the framework of the distorted-wave impulse approximation (DWIA). In DWIA the amplitude of the reaction has three input ingredients: (i) the structural information contained in the transition densities which describe the response of the nuclear system to an external field, (ii) the effective interactions between the projectile and target nucleons, and (iii) the distorted waves describing the relative motion of projectile (ejectile) and target (residual) nucleus.

In addition, it is necessary to take into account the identity of the nucleons in the collision partners, which brings nonlocality to the reaction amplitude. For calculations of this amplitude, nonlocal transition densities would, in principle, be needed. The contribution of exchange knock-out amplitudes can, however, be approximated in the pseudopotential approach.[22] In that approximation, the nonlocal amplitude is reduced to a local one; hence, the local densities discussed above can be used in our cross-section calculations. The effective NN interaction was taken from Ref. 23 (t-matrix interaction describing the free N scattering) and contains central, tensor, and spin-orbit components.

The optical potential used for calculating distorted waves was computed in a ρt-folding model,[23] where ρ is the matter density of ^{6}Li calculated above. The central part of the optical potential was derived from the $S=0$, $T=0$ component of the NN forces. It is well known[24,25] that, in this channel, there are essential corrections due to the influence of the nuclear medium which creates the ρ dependence of the effective NN forces. The ρ depen-

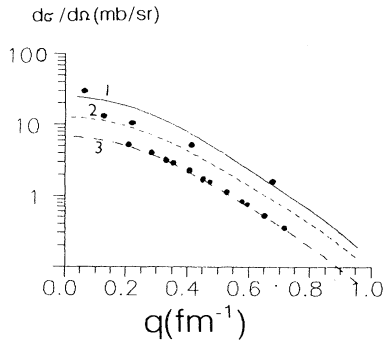

FIG. 5. Comparison between self-consistent DWIA calculations and experimental data (Ref. 26) at $E_{p(n)}=280$ MeV. Curve 1, (p,n); 2, (n,p); and 3, (p,p') reactions.

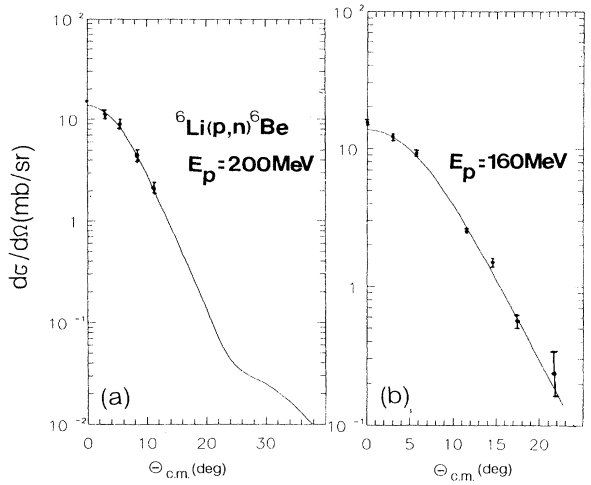

FIG. 6. Same as in Fig. 5 for (p,n) at (a) $E_p=200$ MeV and (b) $E_p=160$ MeV. Experimental data are from Ref. 27.

dence of the effective forces was introduced in the evaluations of the optical potentials by the simple prescription suggested in Ref. 24. The spin-orbital part of the optical potential was evaluated without a ρ-dependent $l\cdot s$ component of the t-matrix interaction.

Thus, our results correspond to "self-consistent" microscopic DWIA calculations of quasielastic reactions, with ingredients tested against available weak and electromagnetic data as discussed above. In this sense there are no free parameters.

The self-consistent evaluations of cross sections reproduce experimental behavior reasonably well up to transferred momentum $q \leq 1$ fm^{-1} for (p,p'), (p,n), and (n,p) reactions on ^{6}Li, populating the isospin triplet.

Results are given in Fig. 5 for the reactions ^{6}Li$(p,n)^6$Be, ^{6}Li$(n,p)^6$He, and ^{6}Li$(p,p')^6$Li$(0^+, 3.56$ MeV) at $E_p=280$ MeV. The experimental data were taken from Ref. 26. The description of inelastic scattering and of the (p,n) reaction is very good. Figure 6 shows differential cross sections for the reaction ^{6}Li$(p,n)^6$Be at somewhat lower energies, $E_p=200$ and 160 MeV, respectively. The experimental data are taken from Ref. 27. The description of the experimental angular distribution is rather good.

VII. SUMMARY AND OUTLOOK

A microscopic three-body formalism based on the hyperspherical harmonics method and fundamental pair interactions has been outlined and shown to have advantages such as a controlled computational accuracy related to a specific approximate three-body symmetry. This feature also allows one to use analytic representations for most of the physical observables. In conjunction with a microscopic nuclear reaction theory, a powerful tool is available for investigating clustering phenomena in lighter nuclei and nuclear reaction mechanisms.

By checking in a self-consistent manner against a variety of characteristics, the ^{6}Li magnetic moment, the ft value of ^{6}He, electromagnetic $M1$ transitions in ^{6}Li, electron scattering from ^{6}Li, and data on ^{6}He fragmentation[28] (which is now available due to experiments with radioactive beams[29]), the quality of our calculated wave functions for ^{6}He and ^{6}Li was found to be rather good. The fact that the $M1$ inelastic and elastic form factors describe experimental data well gives confidence to the calculated transition densities.

To further check these densities, in a self-consistent manner, microscopic DWIA calculations were done for (p,n), (n,p), and (p,p') reactions on ^{6}Li, populating the isospin triplet. For a range of projectile energies, a good fit to data was obtained up to transfered momentum $q \leq 1$ fm^{-1}. It would be very interesting to have data taken for $q \geq 1$ fm^{-1} for further checks.

Other possibilities for testing the accuracy of the transition densities are to study the charge-exchange reactions $A(^6\text{Li},^6\text{He})B$ and $A(^6\text{Li},^6\text{Be})C$ for nuclei A, B, and C of well-known structure and a well-established reaction mechanism.[30]

We have emphasized the dual role of quasielastic reactions (charge-exchange, breakup, single-particle, cluster transfers, etc.) (i) as tools for evaluating the quality of descriptions of few-cluster systems, and (ii) as means for probing structure and reaction mechanisms for heavy nuclei by using known few-body systems as projectiles. The latter is of particular interest in connection with the relative role of proton and neutron degrees of freedom in heavier systems.

A unique possibility to investigate double-charge-exchange mechanisms, for example (^{6}He,^{6}Be), and the unusual space structure of ^{6}He (dineutron and cigarlike components) due to the Pauli focusing phenomenon, now exists with the availability of radioactive beams.

ACKNOWLEDGMENTS

We are grateful to C. Gaarde and N. Shul'gina for useful discussions. F.A.G. is thankful for the hospitality of the Manne Siegbahn Institute (Stockholm) and University of Bergen where part of the work was done. B.D., M.Z., and J.S.V. acknowledge support from The Niels Bohr Institute and NORDITA during a visiting period in Copenhagen.

[1]F. A. Gareev, S. N. Ershov, A. A. Ogloblin, and S. B. Sakuta, Fiz. Elem. Chastits At. Yadra **20**, 1293 (1989) [Sov. J. Part. Nucl. **20**, 541 (1989)].
[2]F. Ajzenberg-Selove, Nucl. Phys. **A413**, 1 (1984).
[3]J. M. Bang and C. Gignoux, Nucl. Phys. **A313**, 119 (1979).
[4]H. R. Weller and D. R. Lehman, Annu. Rev. Nucl. Part. Sci. **38**, 563 (1988).
[5]W. C. Parke and D. R. Lehman, Phys. Rev. C **29**, 2319 (1984).
[6]A. Eskandarian, D. R. Lehman, and W. C. Parke, Phys. Rev. C **38**, 234 (1988).
[7]V. I. Kukulin, V. M. Krasnopol'sky, V. T. Voronchev, and P. B. Sasonov, Nucl. Phys. **A453**, 609 (1986).
[8]J. M. Bang and F. A. Gareev, Nucl. Phys. **A232**, 45 (1974).
[9]B. V. Danilin, M. V. Zhukov, L. V. Chulkov, A. A. Korsheninnikov and V. D. Efros, Yad. Fiz. **49**, 351 (1989) [Sov. J. Nucl. Phys. **49**, 217 (1989)]; **49**, 360 (1989) [**49**, 223 (1989)].
[10]B. V. Danilin, M. V. Zhukov, L. V. Chulkov, and A. A. Korsheninnikov, Yad. Fiz. [Sov. J. Nucl. Phys.] (in press).
[11]S. Ali, A. A. Z. Ahmad, and N. Ferdous, Rev. Mod. Phys. **57**, 923 (1985).
[12]D. Gogny, P. Pires, and R. DeTourreil, Phys. Lett. **32B**, 591 (1970).
[13]L. V. Chulkov, B. V. Danilin, A. A. Korsheninnikov, M. V. Zhukov, and V. D. Efros, Europhys. Lett. **8**, 245 (1989).
[14]B. V. Danilin, M. V. Zhukov, L. V. Chulkov, A. A. Korsheninnikov, and V. D. Efros, Yad. Fiz. **48**, 1208 (1988) [Sov. J. Nucl. Phys. **48**, 766 (1988)].
[15]J. Raynal and J. Revai, Nuovo Cimento A **68**, 612 (1970).
[16]D. A. Varshalovich, A. N. Moskalev, and V. K. Xersonskij, *Quantum Theory of Angular Momentum* (Nauka, Moscow, 1987).
[17]I. C. Bergstrom, S. B. Kowalski, and R. Neuhausen, Phys. Rev. C **25**, 1156 (1982); Nucl. Phys. **A327**, 439 (1979).
[18]R. A. Eramzhyan, G. G. Ryshikh, V. I. Kukulin, and Yu. M. Tchuvil'sky, Phys. Lett. B **228**, 1 (1989).
[19]D. R. Lehman and W. C. Parke, Few Body Syst. **1**, 193 (1986).
[20]W. Jaus and G. Rasche, Phys. Rev. D **35**, 3420 (1987).
[21]Yu. V. Gaponov, N. B. Shul'gina, and P. E. Spivak, Institute of Atomic Energy Report IAE-5032/2; D. Dubbers, W. Mampe, and J. Dohner, Europhys. Lett. **11**, 195 (1990).
[22]F. Petrovich *et al.*, Phys. Rev. Lett. **22**, 895 (1969); W. G. Love, Nucl. Phys. **A312**, 160 (1978).
[23]M. A. Franey and W. G. Love, Phys. Rev. C **31**, 488 (1985).
[24]J. J. Kelly, in *The Interaction Between Medium Energy Nucleons in Nuclei (Indiana Cyclotron Facility, Bloomington, Indiana),* Proceedings of the Workshop on the Interactions Between Medium Energy Nucleons in Nuclei, AIP Conf. Proc. No. 97, edited by Hans-Otto Meyer (AIP, New York, 1982).
[25]F. A. Brieva and J. R. Rook, Nucl. Phys. **A297**, 206 (1978); H. V. Von Geramb, in *The Interaction Between Medium Energy Nucleons in Nuclei* (Ref. 24); K. Nakayama and W. G. Love, Phys. Rev. C **38**, 51 (1988).
[26]O. Hausser *et al.*, Phys. Rev. C **37**, 1119 (1988).
[27]J. Rapaport *et al.* (unpublished).
[28]M. V. Zhukov, B. V. Danilin, A. A. Korsheninnikov, and L. V. Chulkov, Europhys. Lett. **12**, 307 (1990); and (to be published).
[29]T. Kobayashi *et al.*, Phys. Rev. Lett. **80**, 2599 (1988).
[30]A. S. Dem'yanova, J. M. Bang, F. A. Gareev, S. A. Goncharov, S. H. Ershov, A. A. Ogloblin, and P. P. Korovin, Nucl. Phys. **A501**, 336 (1988).